Monte Carlo examination of first-order phase transitions in a system with many independent order parameters: Three-dimensional Ashkin-Teller model

Grzegorz Musiał,* Dorota Jeziorek-Knioła, and Zbigniew Wojtkowiak
Faculty of Physics, A. Mickiewicz University, ul. Uniwersytetu Poznańskiego 2, 61-614 Poznań, Poland

(Received 17 July 2020; revised 10 May 2021; accepted 21 May 2021; published 14 June 2021)

A Monte Carlo (MC) computer experiment for the analysis of first-order temperature-driven phase transitions in a system with one or many independently behaving order parameters is presented using the example of the three-dimensional (3D) Ashkin-Teller model, one of the important reference systems in statistical physics showing a rich and complex phase diagram. The properties of a number of quantities, such as magnetization, three types of cumulants, the internal energy, and its histogram, are exploited. The Lee and Kosterlitz concept proposed for strong first-order phase transitions in systems with one independent order parameter is significantly expanded to obtain results with comparable error bars in reasonable computation times at an arbitrary amount of latent heat. The proposed computer MC experiment uses parallel processing and both the Metropolis and recently formulated cluster algorithms. Arbitrarily weak to strong first-order phase transitions in the phase diagram region with ferromagnetic interactions are investigated and the latent heat associated with individual degrees of freedom is carefully computed. In the discussion of results, the behavior of our 3D system between that of the mean-field and that of the 2D one is bracketed and the role of the Potts point is clarified.

DOI: 10.1103/PhysRevE.103.062124

I. INTRODUCTION

The Ashkin-Teller (AT) model [1] is one of the most important models in statistical physics of current interest. Every year a dozen or so works are devoted to it (see, e.g., the recent papers [2–6] and the ones cited therein), as it is a nontrivial generalization of the widely exploited Ising model. Like the Ising one, the AT model still finds new interesting applications, for example, recently for modeling of the crystalline order in VO_2 [7], machine learning [8], the gapless Coulomb state [9], nanodomain patterns in ultratetragonal $PbTiO_3$ [10], magnetic properties of nanotubes [11], and the elastic response of the DNA molecule to external force and torque [12], among many others.

Initially, the AT lattice model has been proposed for four-component mixture [1], but the interest in it essentially increased after the work by Fan [13], who expressed it in terms of two Ising models put on the same lattice with spins s_i and σ_i at each lattice site i. As in the standard Ising model, we take into account only two spin interactions of a constant magnitude J_2 between the nearest neighbors. These two independent Ising models are coupled by the four-spin interaction of a constant magnitude J_4, also only between couples of nearest-neighboring spins, leading to the effective Hamiltonian H,

$$-\frac{H}{k_BT}=\sum_{[i,j]}\{K_2(s_is_j+\sigma_i\sigma_j)+K_4s_i\sigma_is_j\sigma_j\}. \qquad (1)$$

Here $K_n=-J_n/k_BT$, with $n=2$ or 4, $[i,j]$ denotes the summation over the nearest-neighboring lattice sites, k_B is the Boltzmann constant, and T is the temperature of the system. We consider the symmetric three-dimensional (3D) AT model, i.e., the one with the same interactions between s and σ spins, distributed in the cubic lattice.

This model leads to the $K_2(K_4)$ rich and complex phase diagram because not only can two order parameters, $\langle s\rangle$ and $\langle\sigma\rangle$, induce ordering, but also the product $\langle s\sigma\rangle$ exhibits independent ordering, where the symbol $\langle\ldots\rangle$ denotes the thermal average.

The first systematic study of the phase diagram of the 3D AT model on a cubic lattice, whose current state of knowledge is summarized in Fig. 1, was done by Ditzian *et al.* [14]. Although they exploited short series expansion and Monte Carlo (MC) simulations with very small samples, they were able to sketch the approximate phase diagram, which is an important point of reference, but their results are ambiguous, mainly in the mixed phase region labeled $\langle\sigma\rangle$ in Fig. 1. In the $\langle\sigma\rangle$ region, $\langle s\sigma\rangle=0$ and either $\langle s\rangle$ or $\langle\sigma\rangle$ is ferromagnetically ordered but the other is not. Although a few papers have been published [15–17] that relate to this region, their results are preliminary and it still constitutes a real challenge. The most space in the phase diagram in Fig. 1 is occupied by the Baxter and paramagnetic (labeled "para") phases for which all order parameters, $\langle s\rangle$, $\langle\sigma\rangle$, and $\langle s\sigma\rangle$, are ferromagnetically ordered and are 0, respectively. For phases labeled $\langle s\sigma\rangle_{\rm F}$ and $\langle s\sigma\rangle_{\rm AF}$, $\langle s\rangle=\langle\sigma\rangle=0$ and only the parameter $\langle s\sigma\rangle$ is ferromagnetically and antiferromagnetically ordered, respectively. The dotted curves denote the first-order phase transitions, whereas the solid curves denote the continuous ones. The positions of labeled points are marked by crosses. A, F, G, H, H′, K, and K′ are the tricritical points. The first more precise results were obtained by Arnold and Zhang [18] along the line AP using MC simulations. Ising phase transitions occur along the continuous curves ending at the tricritical points K

*gmusial@amu.edu.pl

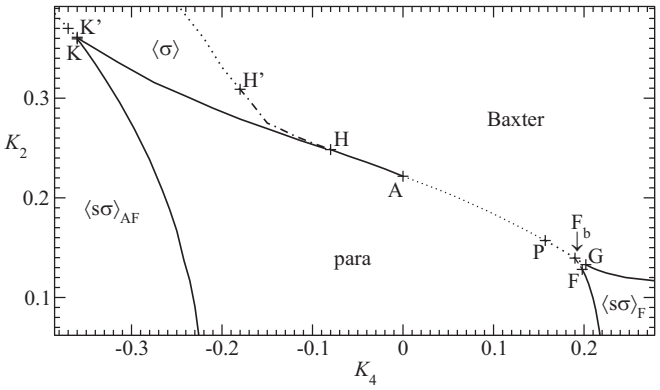

FIG. 1. Phase diagram of the symmetric 3D AT model on a cubic lattice. Dotted curves denote first-order phase transitions, solid curves represent continuous transitions, and the dotted-dashed curve indicates transitions of both types for different order parameters. In the phase labeled "Baxter" the system is ferromagnetically ordered with all order parameters $\langle s\rangle$, $\langle\sigma\rangle$, and $\langle s\sigma\rangle$ nonzero, whereas in the phase labeled "para" they are all 0. In the phases $\langle s\sigma\rangle_{\rm F}$ and $\langle s\sigma\rangle_{\rm AF}$, $\langle s\rangle = \langle\sigma\rangle = 0$, and only the order parameter $\langle s\sigma\rangle$ is ferromagnetically and antiferromagnetically ordered, respectively. For phase $\langle\sigma\rangle$, called the mixed phase region, $\langle s\sigma\rangle = 0$ and either $\langle s\rangle$ or $\langle\sigma\rangle$ is ferromagnetically ordered but the other is not. The positions of labeled points within the phase diagram are marked by crosses and A, F, G, H, H′, K, and K′ are the tricritical points.

and F [19–21]. However, this character has not been clearly confirmed for the continuous curve ending at the tricritical point G [20]. Thus, the phase diagram of the AT model in three dimensions is much more complex than the much better studied diagram in two dimensions, where only continuous phase transitions occur, and instead of the mixed phase region there is a continuation of the paramagnetic phase (see, e.g., [3,14,22], and the papers cited therein).

For these reasons, this model is difficult to analyze also using computer methods, but one can bracket the behavior of our 3D system between that of the 2D one and that of the mean-field one. The former shows the interesting line of continuously varying phase transitions at $K_4 \leqslant K_2$ first shown in Ref. [23], which starts at the Potts point with $K_4 = K_2$. At this point, the AT model reduces to the four-state Potts model, which in two dimensions exhibits a continuous phase transition but in three dimensions shows a first-order one [24]. MC simulation results suggest the possibility of the occurrence of nonuniversal behavior also in the 3D AT model [14–17,19,22] but recent results indicate only a wide crossover along the AH line and the rare coexistence of continuous and first-order phase transitions along the HH′ line [22] shown in Fig. 1. However, the character of continuous phase transitions along the HK′ line is still an open question. Similarly, studying the region covering the boundary between phase $\langle s\sigma\rangle_{\rm AF}$ and phase $\langle\sigma\rangle$ remains a challenge. However, our preliminary results obtained using the method proposed in this study are encouraging.

In this paper, we present our large-scale MC computer experiment to study first-order temperature-driven phase transitions in a system with one or many order parameters showing independent ordering, which is demonstrated with the example of the symmetric 3D Ashkin-Teller model. We exploit the properties of various cumulants and the internal energy histogram, but in contrast to Ref. [25] we do not limit our study to strongly first-order phase transitions. Since completing all our results requires over a thousand runs of our computer programs, we use samples of size L^3, mainly with L up to 40, which allows us to obtain results with the assumed accuracy of four significant digits within a reasonable time.

To demonstrate the wide possibilities of the proposed method, we have investigated the broad and interesting region of the phase diagram along the line APF_b between the Baxter and the paramagnetic phases, where phase transitions of the first order from arbitrarily weak to strong are signaled [18,26]. Precise determination of the position of a phase transition point and computation of latent heat values associated with individual order parameters, i.e., with individual terms in Hamiltonian (1), in the considered system are of key importance here and enable us to complete a planned study of mixed phase region $\langle\sigma\rangle$. This allowed us to verify the region where the phase transitions related to the individual order parameters occur along the same APF_b curve within the limits of error bars, as well as the location of the bifurcation point F_b. As in the 2D system the interesting line of continuously varying phase transitions starts at the Potts point, which is the point of bifurcation; we have clarified the role of the Potts point P in the 3D case where the bifurcation point is F_b as shown in Fig. 1.

II. THE MC COMPUTER EXPERIMENT

We exploit the MC computer experiment with importance sampling of states. The finite-size cubic samples of the lattice symmetric AT model defined in Hamiltonian (1) are considered, and they are sufficiently large to be able to compute the thermodynamic limit of our results. When performing our MC computer experiments, we not only compute the thermodynamic quantities but also carefully determine their error bars.

In this way, we perform our computer experiments to predict the equilibrium behavior of our model according to the statistical mechanics methodology. The behavior of our system is fully determined by Hamiltonian (1). Due to the presence of metastable and unstable states [3], we generate equilibrium configurations (also called microstates) of finite-size cubic spin samples $L \times L \times L$ for fixed values of our model parameters described above in Hamiltonian (1) using our cluster algorithm of the Wolff type [27] in the critical region and the Metropolis one beyond. This is the best strategy, also, to obtain results with comparable uncertainties in a shorter time.

Periodic boundary conditions are assumed. We apply thermalization of the length of the order of 10^6 Monte Carlo steps (MCSs). This in excess is enough to bring the system to thermodynamic equilibrium, because for the largest samples for simulations using the Metropolis scheme, the integrated autocorrelation time is less than 10^6, and for our Wolff-type cluster algorithm, it is several orders of magnitude smaller (see Fig. 9 in our previous paper [27]). Moreover, one MCS in our computer experiment is completed when the accumulated number of attempts at flip spins reaches the number of spins in the lattice. We split each MC run into k $(6 \leqslant k \leqslant 20)$

segments called partial averages to determine the uncertainties of the computed quantities. One partial average consists of 0.4×10^6 MCSs for the smallest system sizes up to 3.6×10^6 MCSs for the largest L's and only every 8th to 10th MCS contributes to the computation of the partial averages, which is quite sufficient for the partial averages to be uncorrelated [27]. We have increased the number of MCSs to 10^9 to test that the values of the computed quantities remain the same and only the error bars decrease slightly. Hence we conclude that the number of MCSs is sufficient for the system to repeatedly tunnel from one phase to the other in a first-order phase transition region.

One run of our MC computer experiment takes from 20 h for the smallest L's up to a couple of months for the largest L values considered, when sequential processing is applied. Therefore, to obtain the results in a reasonable time, we have parallelized the processing in our computer experiment [28]. Thousands of such runs have been executed to complete the results presented in this paper.

First, we fix a particular value of K_4 coupling and analyze Binder cumulant $Q_{\alpha,L}(K_2) = \langle M_\alpha^2 \rangle_L^2 / \langle M_\alpha^4 \rangle_L$ dependences to prelocate a temperature-driven phase transition point (see, e.g., [20–22,29]). $\langle M_\alpha^n \rangle_L$ denotes the nth power of the order parameter α, with $\alpha = s$, σ, or their product $s\sigma$, which are averaged over an ensemble of independent samples of size $L \times L \times L$. The presence of characteristic minima in the course of the $Q_{\alpha,L}(K_2)$ dependences indicates that the phase transition can be of first order [17,29].

To unambiguously determine the character of a phase transition and for a more precise location of a phase transition point, we compute also the Challa-like [30]

$$V_{\alpha,L} = 1 - \frac{\langle E_\alpha^4 \rangle_L}{3 \langle E_\alpha^2 \rangle_L^2} \tag{2}$$

and the Lee-Kosterlitz-like [25]

$$U_{\alpha,L} = \frac{\langle E_\alpha^2 \rangle_L}{\langle E_\alpha \rangle_L^2} \tag{3}$$

cumulants. $\langle E_\alpha^n \rangle_L$ is the nth moment of the interaction energy of α degrees of freedom ($\alpha = s$, σ, or their product $s\sigma$) in Hamiltonian (1) separately, which is averaged over an ensemble of independent samples of size $L \times L \times L$. We have adapted the Challa and Lee-Kosterlitz cumulants by taking not only the whole Hamiltonian (1) for the energy E as originally proposed by Challa *et al.* [30] and by Lee and Kosterlitz [25], but also the Hamiltonian individual terms, to be able to compute the latent heat l_α for each order parameter $\langle \alpha \rangle$ separately [19,22,26].

The dependences $V_{\alpha,L}(K_2)$ show characteristic local minima [30] and $U_{\alpha,L}(K_2)$ characteristic local maxima [25] at a fixed value of K_4 coupling in the close critical region for first-order phase transitions. Our cumulant values as a function of K_2 were approximated by a fourth-degree polynomial in the close extremum region to average the scatter of our results and to determine more precisely the abscissa and the ordinate of the extremum under consideration. For this purpose, we have exploited the fourth-degree polynomial regression analysis, which gave us the respective values together with their error bars.

The latent heat l_α coming from the above-mentioned interaction energy E_α of the α order parameter in the limit $L \to \infty$

$$l_\alpha = E_{\alpha,+} - E_{\alpha,-}, \tag{4}$$

where $E_{\alpha,\pm} = E_\alpha(K_2 \to K_{2,c}|_\pm)$, is determined on the basis of the Lee-Kosterlitz formula [25,31]

$$V_{\alpha,L}^{\min} = \frac{2}{3} - \frac{1}{12}\left(\frac{E_{\alpha,+}}{E_{\alpha,-}} - \frac{E_{\alpha,-}}{E_{\alpha,+}}\right)^2 + \frac{A_V}{L^3} \tag{5}$$

and using the method proposed in [19]. It should be noted that Eq. (5) was also obtained independently by Borgs, Kotecky, and Miracle-Sole [32] from a more rigorous point of view. Derivation of this equation [25] exploits general thermodynamic properties and is not limited to a specific form of the expression for the energy. Here $K_{2,c}$ is the critical value of K_2 coupling with the fixed value of K_4. The quantity A_V in Eq. (5) stands for L independent expression of the complicated form [25]. Thus, Eq. (5) allows us to determine the $V_{\alpha,\infty}^{\min}$ limit value using linear regression to analyze our $V_{\alpha,L}^{\min}(L^{-3})$ computer experiment data. This method is a powerful tool and a similar analysis has been applied to first-order phase transitions with an exponential low-temperature phase degeneracy [33].

Similarly, we determine the latent heat l_α using the $U_{\alpha,L}$ cumulant maximum values scaled to the thermodynamic limit for each of the three α order parameters independently, as well as for the whole system (which we denote $\alpha = H$), using the Lee-Kosterlitz formula [25]

$$U_{\alpha,L}^{\max} = \frac{(E_{\alpha,+} + E_{\alpha,-})^2}{4E_{\alpha,+}E_{\alpha,-}} + \frac{A_U}{L^3}, \tag{6}$$

where A_U stands for the L independent complicated expression.

Thus, the values and locations of cumulant $V_{\alpha,L}$ minima and of cumulant $U_{\alpha,L}$ maxima scale linearly versus L^{-3}. We conclude that when the thermodynamic limit $V_{\alpha,L}^{\min}$ value with its error bar remains different from 2/3 and the $U_{\alpha,L}^{\max}$ value with its error bar remains different from 1, a phase transition is qualified to be of the first order; otherwise we assume that the phase transition is continuous [19,22,25,30]. Naturally, the thermodynamic limit $K_{2,\alpha}^{\min}$ values of minima and $K_{2,\alpha}^{\max}$ values of maxima are better estimations of the critical K_2 values than the ones obtained on the basis of the Binder cumulant $Q_{\alpha,L}(K_2)$ dependences mentioned above.

Thanks to the use of cumulants, we can locate a point of phase transition with sufficient accuracy to be able to use another independent method of computing the latent heat with greater accuracy. For sufficiently strong first-order phase transitions, a characteristic histogram of the internal energy E_α distribution with two peaks in the close critical region can be observed [25,34,35]. For samples of finite-size L, the maxima of these peaks appear at the energy value $E_{\alpha,-,L}$ for the ordered state and at $E_{\alpha,+,L}$ for the unordered one. Thus, we compute the probability $P_{\alpha,L}$ of the energy $E_{\alpha,L}$ appearance in the system of finite size L^d, with dimensionality $d = 3$ here. As in the case of cumulants, the $P_{\alpha,L}(E_{\alpha,L})$ values are computed independently for each degree of freedom $\alpha = s$, σ, or their product $s\sigma$ and, also, for the whole Hamiltonian (1), denoted $\alpha = H$, at a critical value $K_{2,c}$. It is noteworthy

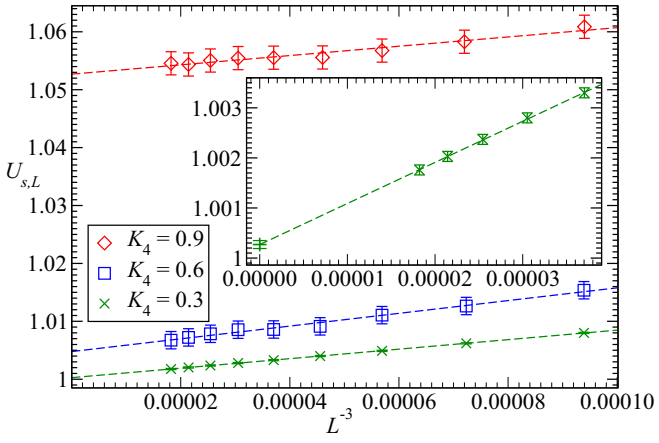

FIG. 2. The values of Lee-Kosterlitz-like cumulant maxima $U_{\alpha,L}^{\max}$ extrapolated to the thermodynamic limit for $\alpha = s$ at the fixed values of the coupling $K_4 = 0.03$, 0.06, and 0.09 are represented by symbols explained in the legend. The dependences are fitted by straight dashed lines using linear regression. The symbol + in the inset indicates the exemplary result of this extrapolation for $K_4 = 0.03$.

that for continuous phase transitions only a single peak of the probability $P_{\alpha,L}(E_{\alpha,L})$ dependence appears in the thermodynamic limit.

To obtain reliable results in this method, we carefully check whether the results we have obtained independently on the basis of some cumulants based on the order parameter and of other cumulants based on the internal energy, as well as on the internal energy distribution histogram, are consistent within the error bars.

III. RESULTS AND CONCLUSIONS

As explained in the previous section, we have first prelocated temperature-driven phase transition points along the line APF_b at fixed values of the coupling K_4 on the basis of the Binder cumulant [29] curves $Q_{\alpha,L}(K_2)$. These analyses have been performed independently for $\langle\alpha\rangle$ order parameters with $\alpha = s, \sigma$, and $s\sigma$ (see, e.g. [19,20,22]), allowing us to estimate four decimal digits of the K_2 coupling critical value $K_{2,c}$. For a particular K_4 value, these three $K_{2,c}$ values are consistent within the limits of their error bars along the entire APF_b line.

One of the essential results presented in this paper is the latent heat computed for each of the three differently behaving order parameters as well as for the whole system. For this purpose, we have first exploited the Challa-like $V_{\alpha,L}$ and the Lee-Kosterlitz-like $U_{\alpha,L}$ cumulant properties explained in the previous section.

An example of such analyses is shown in Fig. 2 for the Lee-Kosterlitz-like $U_{s,L}$ cumulant for $16 \leqslant L \leqslant 32$ at fixed values of the coupling $K_4 = 0.03$, 0.06, and 0.09 indicated in the legend. To compute the latent heat, we have first estimated the values of the cumulant $U_{s,L}$ maxima in the thermodynamic limit using linear regression for $U_{s,L}^{\max}(L^{-3})$ dependences, which follows from Eq. (6). The symbol + in the inset indicates the example result of this extrapolation for $K_4 = 0.03$, which is $U_{s,\infty}^{\max} = 1.000\,27(8)$, while for $K_4 = 0.06$ and 0.09 we have obtained $U_{s,\infty}^{\max} = 1.0048(15)$ and 1.0527(24), respectively. One can see the clear linear character of our MC computer experiment data, but the higher the $U_{s,\infty}^{\max}$ values, i.e., the higher the latent heat, the greater the statistical scatter of the results and their error bars, which is in line with expectations. In this way, we have determined the cumulant $V_{\alpha,\infty}^{\min}$ and $U_{\alpha,\infty}^{\max}$ values together with their error bars in the thermodynamic limit for individual $\langle\alpha\rangle$ order parameters along the entire APF_b line, where $\alpha = s, \sigma, s\sigma$, or H, where H denotes the result obtained when applying the energy of the whole system with the Hamiltonian H given in Eq. (1).

We have independently determined the $E_{\alpha,-}$ value by equating the $V_{\alpha,\infty}^{\max}$ or $U_{\alpha,\infty}^{\min}$ values to the constant terms in Eq. (5) or (6), respectively, and taking into account the value $E_{\alpha,+}$ estimated from the $E_{\alpha,L}(K_2)$ energy plot for the finite-size samples [19,22]. Although such computation of the step change from E_+ to E_- of the energy in the thermodynamic limit during the transition from the disordered phase to the Baxter one seems imprecise, it enables both the calculation of the values $E_{\alpha,+}$ and $E_{\alpha,-}$ and a qualitative verification of the location of this energy value jump against the background of the course of the dependences $E_{\alpha,L}(K_2)$. The value of this estimation is increased by the fact that such a computed $E_{\alpha,-}$ value is slightly dependent on the accuracy of the estimation of the $E_{\alpha,+}$ value that varies only in the third significant digit place [19,22]. Having the values of $E_{\alpha,+}$ and $E_{\alpha,-}$ obtained in this way on the basis of the values of $V_{s,\infty}^{\max}$ and $U_{s,\infty}^{\min}$ introduced in Eq. (4) we have obtained $l_{\alpha,V}$ and $l_{\alpha,U}$ values, where $\alpha = s, \sigma, s\sigma$, or H, for individual K_4 values along the APF_b line. The indexes V and U indicate cumulants, on the basis of which the latent heat was computed. For example, taking the values obtained from Fig. 2 for $K_4 = 0.03$, 0.06, and 0.09, we have obtained $l_{s,U} = 0.0058(21)$, 0.0269(12), and 0.0734(9) in k_BT units, respectively.

Although Eq. (5) has been derived for strong first-order phase transitions, our careful analyses show that it gives correct results for both strong and weak ones, in line with the more rigorous derivation of Eq. (5) obtained by Borgs *et al.* [32], which does not exclude its application to weak phase transitions. The stronger the phase transitions, the greater the area under the probability peak on the ferromagnetically ordered phase side, which justifies the assumption of Lee and Kosterlitz that the weights should be different in the combination of two Gaussians which approximate the probability distribution. It is also worth emphasizing here that although the weaker the transition, the closer the probability peaks are, their analysis is possible with sufficiently large system sizes L. With the moderate values of L mentioned in the third paragraph in Sec. II, using the cumulants, we could perform analyses up to $K_4 = 0.03$, where the value of the latent heat $l_{H,V}$ in k_BT units is only 0.0066(15), and even up to $K_4 = 0.01$, where $l_{H,V} = 0.0016(55)$, which is compatible with 0 within the error bar [26].

The abscissas $K_{2,\alpha,L}^{\min}$ of the $V_{\alpha,L}(K_2)$ dependence minima and the abscissas $K_{2,\alpha,L}^{\max}$ of the $U_{\alpha,L}(K_2)$ dependence maxima at a fixed value of the coupling K_4 also are linearly correlated with L^{-3} [19,22,25,30]. Scaling the positions of these extremes to their thermodynamic limits, we have determined $K_{2,\alpha,\infty}^{\min}$ and $K_{2,\alpha,\infty}^{\max}$ values, respectively, which more accurately locate the phase transition point, i.e., the critical value of $K_{2,\alpha}$, as explained in the previous section. The $K_{2,\alpha,\infty}^{\min}$ and $K_{2,\alpha,\infty}^{\max}$

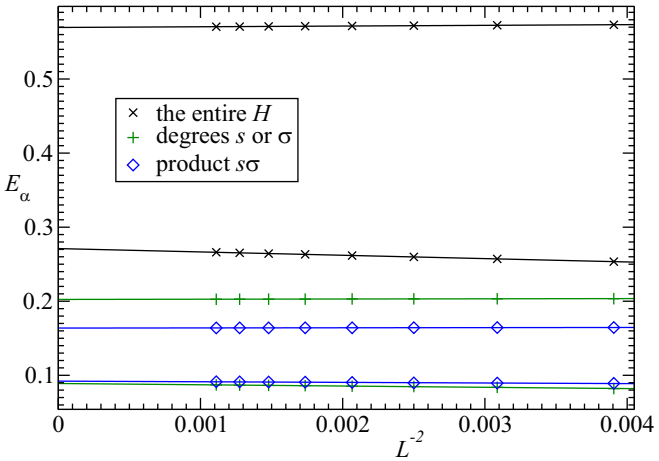

FIG. 3. Values of $E^{\min}_{\alpha,+,L}$ (upper lines) and $E^{\min}_{\alpha,-,L}$ (lower lines) in k_BT units of the minima of dependencies $-\ln P_{\alpha,L}(E_{\alpha,L})$ obtained for the phase transition at $K_4 = 0.12$ and $K_{2,c} = 0.174\,90(4)$ for the system of finite size L and for the items α explained in the legend. The individual lines are extrapolated to their thermodynamic limit $E_{\alpha,+}$ or $E_{\alpha,-}$ using linear regression.

values, as well as the critical $K_{2,\alpha}$ values predetermined on the basis of the cumulant $Q_{\alpha,L}(K_2)$ dependences, are the same within the error bars at a particular K_4 value along the entire APF$_b$ line. We denote as $K_{2,c}$ the average value calculated from all critical values of $K^{\min}_{2,\alpha,\infty}$ and $K^{\max}_{2,\alpha,\infty}$ at a fixed K_4 value.

The results obtained so far are based on independent analyses of the dependences of three different cumulants Q, V, and U on the coupling constant K_2 at a fixed value of K_4. In this way, we have located the phase transition points precisely enough to be able to use another independent method. For sufficiently strong first-order phase transitions, we have obtained completely independent confirmation of the correctness and the increased accuracy of our results thanks to the internal energy E_α distribution histogram analyses [22,25,34] with $\alpha = s$, σ, $s\sigma$, and also H. Also, here H means that we have assumed the entire Hamiltonian [specified in Eq. (1)] as the energy, not the energy of its particular term, as in the case of the first three items. For all α items, we have observed two distinct probability $P_{\alpha,L}$ peaks corresponding to the energies $E_{\alpha,-,L}$ and $E_{\alpha,+,L}$, for the ordered and unordered states, respectively. Locating the phase transition point accurately is crucial for this method [25].

These two probability $P_{\alpha,L}$ peaks correspond to the minima of the $-\ln P_{\alpha,L}(E_{\alpha,L})$ function [25]. We have first determined the energy values corresponding to the lower minima $E_{\alpha,-,L}$ of this function for the ordered state and to the upper minima $E_{\alpha,+,L}$ for the unordered state for all α items specified in the previous paragraph at different values of a finite system size L.

Figure 3 shows the results of our analyses for the energies $E^{\min}_{\alpha,-,L}$ (lower lines) and $E^{\min}_{\alpha,+,L}$ (upper lines) in k_BT units for the energy of interaction of degrees of freedom $\alpha = s$ [the same results are obtained for $\alpha = \sigma$ due to the Hamiltonian (1) symmetry], for the product $s\sigma$ and for the entire Hamiltonian separately, explained in the legend, for the system with different sizes $16 \leqslant L \leqslant 30$ at the critical point $K_4 = 0.12$ and $K_{2,c} = 0.17490(4)$. The values $E_{\alpha,-,L}$ and $E_{\alpha,+,L}$ in the L^{-2} function scale linearly to the respective bulk values $E_{\alpha,-}$ and $E_{\alpha,+}$ [22,25,34]. This agrees with the theoretically derived dependence of the positions of these minima on $1/L^{d-1}$ in the paper by Lee and Kosterlitz [25] [which results from their Eq. (2.3)], where d is the dimension of the system. It should be noted here that the results for the latent heat obtained from the dependence of the positions of these minima on $1/L^3$, i.e., on $1/L^d$ derived in the paper by Billoire, Neuhaus, and Berg [35], as well as on $1/L^{-1}$, are significantly different from the results obtained on the basis of the cumulants V and U; their error bars are disjoint. Therefore, the individual lines in Fig. 3 were extrapolated to their thermodynamic limits using linear regression. The resulting values $E_{s,-} = 0.0900(6)$ and $E_{s,+} = 0.2024(4)$, after substitution into Eq. (4) at $K_4 = 0.12$, gave the latent heat $l_{s,P} = 0.1124(10)$, all in k_BT units here and below. The index P indicates that the latent heat value was obtained on the basis of the dependence $-\ln P_{\alpha,L}(E_{\alpha,L})$ minima. Of course, the results $l_{\sigma,P}$ for degrees of freedom σ are the same because of the symmetry of Hamiltonian (1). Similarly, $E_{s\sigma,-} = 0.0921(6)$, $E_{s\sigma,+} = 0.163\,77(12)$, and $l_{s\sigma,P} = 0.0717(7)$. In this way, we have computed the contributions to the latent heat from all three order parameters. After adding them up, we have obtained $l_{\mathrm{sum},P} = 0.2965(27)$ at $K_4 = 0.12$.

The top two lines in Fig. 3 show the results for the whole system obtained using the energy of the entire Hamiltonian (1), which, extrapolated to the thermodynamic limit, gave $E_{H,-} = 0.271\,08(36)$ and $E_{H,+} = 0.569\,59(24)$. In this way, using Eq. (4), we have found the latent heat of the whole system with the highest accuracy $l_{H,P} = 0.2985(6)$. For our system, it is important to check whether the sum l_{sum} of the contributions l_α to the latent heat from individual $\langle\alpha\rangle$ order parameters is equal to l_H within the limits of error bars, which is well satisfied along the whole line APF$_b$.

Of course, this condition is also satisfied for the latent heat computed above on the basis of analyses of V and U cumulant behavior. For example, at $K_4 = 0.12$, the value of $U^{\max}_{s,\infty} = U^{\max}_{\sigma,\infty} = 1.183(12)$ gives $l_{s,U} = l_{\sigma,U} = 0.1143(23)$, and for $U^{\max}_{s\sigma,\infty} = 1.084(5)$ we have obtained $l_{s\sigma,U} = 0.0713(15)$, therefore $l_{\mathrm{sum},U} = 0.2999(61)$, which, within the error bars, is consistent with $l_{H,U} = 0.2997(27)$ obtained on the basis of $U^{\max}_{H,\infty} = 1.146(4)$. Similarly, $V^{\min}_{s,\infty} = V^{\min}_{\sigma,\infty} = 0.380(6)$ gives $l_{s,V} = l_{\sigma,V} = 0.1130(14)$, from $V^{\min}_{s\sigma,\infty} = 0.546(6)$ we have got $l_{s\sigma,V} = 0.0712(16)$, hence $l_{\mathrm{sum},V} = 0.2972(44)$, which, within the error bars, agrees with $l_{H,V} = 0.2976(20)$ obtained from $V^{\min}_{H,\infty} = 0.449(5)$.

For strong phase transitions, the results of $l_{\alpha,V}$ and $l_{\alpha,U}$ are less accurate, but they are consistent within the error bars with the latent heat $l_{\alpha,P}$ obtained on the basis of the energy histograms. It should be remembered, however, that the energy histogram analysis we use has been derived for strong phase transitions of the first order, as we have indicated in the previous section. Therefore, for $K_4 < 0.06$ and $K_4 > 0.195$, the two minima of the dependencies $-\ln P_{\alpha,L}(E_{\alpha,L})$ become separated by too large values of the system size L to obtain results in a reasonable time. However, due to the smaller amount of latent heat in these ranges of K_4 values, our results $l_{\alpha,V}$ and $l_{\alpha,U}$ obtained on the basis of cumulants V and U have comparable error bars, as expected.

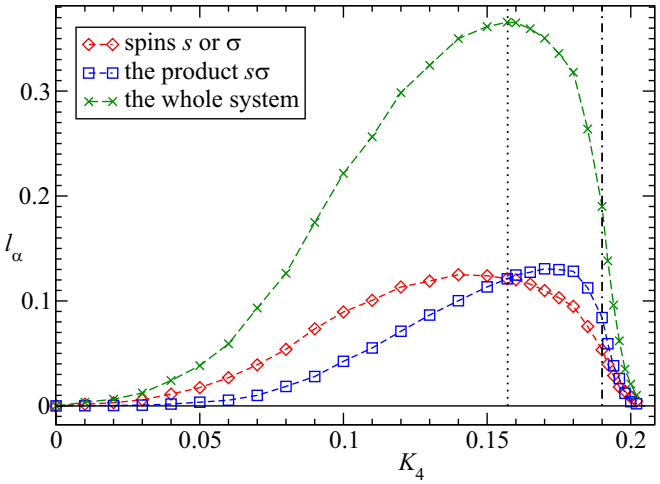

FIG. 4. The dependences of the latent heat l_α values in k_BT units on the coupling constant K_4 values along the APF$_b$ line shown in Fig. 1 for the items α explained in the legend. The lowest position denotes the latent heat for the whole system computed using the entire Hamiltonian (1). The error bars are of the order of the magnitude of symbols. The dotted vertical line indicates the position of the Potts point, while the dotted-dashed line indicates the position of the bifurcation point F$_b$.

This feature is essential for analyses near a point A (see Fig. 1), where the AT model reduces to the Ising model with ferromagnetic interactions limited only to the nearest neighbors. Thus, here phase transitions change their character from first order to continuous. Impressive is the occurrence of arbitrarily weak first-order phase transitions when approaching point A [18], which we have preliminary investigated in our conference paper [26] using only the cumulants Q and V and the Metropolis algorithm. In this paper, we have refined these results by expanding our analysis to include the use of U cumulants and our recently proposed cluster algorithm [27].

Figure 4 illustrates our best latent heat results for phase transitions along the APF$_b$ line using the symbols explained in the legend. We have refined the location of point F$_b$ at $K_4 = 0.190(1)$ and $K_2 = 0.139\,47(4)$ [19], which is represented by the dotted-dashed vertical line in Fig. 4. This line also shows that not only the latent heat l_H but also l_s and $l_{s\sigma}$ at point F$_b$ remain significantly different from 0. The dotted vertical line indicates the position of the Potts point, which in the 2D AT model is the bifurcation point and the beginning of the interesting line of continuously varying phase transitions at $K_4 \leqslant K_2$. As mentioned in Sec. I, one can bracket the behavior of our 3D system between that of the 2D one and that of the mean-field one. The latter predicts [14] that F$_b$ is a bifurcation point, and point P lies inside the first-order phase transition line APF$_b$ without a distinguished role. Figure 4 reveals the role of the Potts point P at $K_4 = K_2 = 0.157\,154$ in the 3D AT model: here the latent heat of the whole system has the highest value $l_H = 0.3657(12)$, while the maximum $l_s = l_\sigma = 0.1250(10)$ occurs at a smaller value, $K_4 = 0.14(1)$, and the maximum $l_{s\sigma} = 0.1306(5)$ at a higher value, $K_4 = 0.17(1)$.

It is noteworthy that for negative K_4 values in Fig. 1, at first there appears a wide crossover effect that covers the whole line between the tricritical points A and H [22] shown in Fig. 1, while the question about the nonuniversal behavior of this model along the HK′ line [15,16] as well as study of the region covering the boundary between phase $\langle s\sigma\rangle_{\rm AF}$ and phase $\langle\sigma\rangle$ remains open and requires further study.

In summary, our MC computer experiment and the method, which is based on analyses of the behavior of a number of quantities, such as magnetization, three different types of cumulants, and the internal energy and its histogram, have been carefully checked. They can successfully be used for the analysis of first-order temperature-driven phase transitions not only in any system with Ising-like degrees of freedom with a single independent order parameter [25], but also in complex systems with many order parameters showing individual ordering as in the AT model. Although completing all our results with the assumed accuracy of four significant digits requires over a thousand runs of our computer programs, they were obtained in a reasonable time, because for this purpose, computations with sample sizes L below 40 are sufficient.

Results of our computer experiments justify that although Eq. (5) has been derived by Lee and Kosterlitz [25] for strong first-order phase transitions, it gives correct results for both strong and weak ones, in line with the more rigorous derivation of Eq. (5) obtained by Borgs *et al.* [32], which does not exclude its application also to weak phase transitions. This conclusion also applies to Eq. (6) derived by Lee and Kosterlitz [25]. Furthermore, only our results for the latent heat $l_{\alpha,P}$ obtained from the dependence of the positions of the minima of the function $-\ln P_{\alpha,L}(E_{\alpha,L})$ on $1/L^{d-1}$ derived by Lee and Kosterlitz [25] are consistent with the results of this heat $l_{\alpha,V}$ and $l_{\alpha,U}$ computed on the basis of cumulants V_α and U_α, respectively, within the error bar limits, while $l_{\alpha,P}$ obtained from the dependence of the positions of these minima on $1/L^d$ derived in the paper by Billoire, Neuhaus, and Berg [35] are significantly different from $l_{\alpha,V}$ and $l_{\alpha,U}$, i.e., their error bars are disjoint.

We have significantly expanded the method of Lee and Kosterlitz proposed for strong first-order phase transitions [25]. We have considered phase transitions from arbitrarily weak to strong, obtaining comparable error bars of the results in similar computation times using the example of one of the basic models in statistical physics. In our computer experiments, not only have we exploited the standard Metropolis algorithm, which shows a critical slowing-down, but also, due to the presence of metastable and unstable states [3], the reliability of the results obtained significantly raises the use of our new Wolff-type cluster algorithm adapted for the Ashkin-Teller model [27]. It is noteworthy that thanks to the basing of our cluster algorithm on the Wolff scheme, the problem of critical slowing-down is practically nonexistent. In contrast, the use of the Swendsen-Wang scheme [36] only partially reduces this problem [37].

ACKNOWLEDGMENTS

Numerical calculations were carried out on the computing platforms of the Poznań Supercomputing and Networking Center as well as the Faculty of Physics at Adam Mickiewicz University in Poznań.

[1] J. Ashkin and E. Teller, Phys. Rev. **64**, 178 (1943).
[2] S.-P. Li and Z.-H. Sun, Phys. Rev. A **98**, 022317 (2018).
[3] J. P. Santos, J. A. J. Avila, D. S. Rosa, and R. M. Francisco, J. Magn. Magn. Mater. **469**, 35 (2019).
[4] G. Delfino and N. Lamsen, J. Phys. A: Math. Theor. **52**, 35LT02 (2019).
[5] P. Patil and A. W. Sandvik, Phys. Rev. B **101**, 014453 (2020).
[6] A. Benmansour, S. Bekhechi, B. N. Brahmi, N. Moussa, and H. Ez-Zahraouy, J. Magn. Magn. Mater. **511**, 166944 (2020).
[7] T. Lovorn and S. K. Sarker, Phys. Rev. Lett. **119**, 045501 (2017).
[8] S. S. Lee and B. J. Kim, Phys. Rev. E **99**, 043308 (2019).
[9] G.-Y. Zhu and G.-M. Zhang, Phys. Rev. Lett. **122**, 176401 (2019).
[10] A. Kumar, J. G. M. Guy, L. Zhang, J. Chen, J. M. Gregg, and J. F. Scott, Appl. Phys. Lett. **116**, 182903 (2020)
[11] R. M. Francisco and J. P. Santos, Phys. Lett. A **383**, 1092 (2019).
[12] C. Zhe, W. Ping, and Z. Ying-Hong, Commun. Theor. Phys. **49**, 525 (2008).
[13] C. Fan, Phys. Lett. A **39**, 136 (1972).
[14] R. V. Ditzian, J. R. Banavar, G. S. Grest, and L. P. Kadanoff, Phys. Rev. B **22**, 2542 (1980).
[15] G. Musiał, Phys. Status Solidi B **236**, 486 (2003).
[16] G. Musiał and J. Rogiers, Phys. Status Solidi B **243**, 335 (2006).
[17] D. Jeziorek-Knioła, G. Musiał, L. Dębski, J. Rogiers, and S. Dylak, Acta Phys. Polon. A **121**, 1105 (2012).
[18] P. Arnold and Y. Zhang, Nuclear Phys. B **501**, 803 (1997).
[19] G. Musiał, Phys. Rev. B **69**, 024407 (2004).
[20] G. Szukowski, G. Kamieniarz, and G. Musiał, Phys. Rev. E **77**, 031124 (2008).
[21] G. Musiał, L. Dębski, and G. Kamieniarz, Phys. Rev. B **66**, 012407 (2002).
[22] Z. Wojtkowiak and G. Musiał, Physica A **513**, 104 (2019).
[23] C. Fan and F. Y. Wu, Phys. Rev. B **2**, 723 (1970).
[24] A. K. Murtazaev and A. B. Babaev, J. Magn. Magn. Mater. **324**, 3870 (2012).
[25] J. Lee and J. M. Kosterlitz, Phys. Rev. B **43**, 3265 (1991).
[26] D. Jeziorek-Knioła, G. Musiał, and Z. Wojtkowiak, Acta Phys. Polon. A **127**, 327 (2015).
[27] Z. Wojtkowiak and G. Musiał, J. Magn. Magn. Mater. **500**, 166365 (2020).
[28] G. Musiał and L. Dębski, Lect. Notes Comp. Sci. **2328**, 535 (2002).
[29] K. Binder and D. P. Landau, Phys. Rev. B **30**, 1477 (1984).
[30] M. S. S. Challa, D. P. Landau, and K. Binder, Phys. Rev. B **34**, 1841 (1986).
[31] K. Binder, Rep. Prog. Phys. **60**, 487 (1997).
[32] C. Borgs, R. Kotecky, and S. Miracle-Sole, J. Stat. Phys. **62**, 529 (1991).
[33] M. Mueller, W. Janke, and D. A. Johnston, Phys. Rev. Lett. **112**, 200601 (2014).
[34] D. Jeziorek-Knioła, Z. Wojtkowiak, and G. Musiał, Acta Phys. Polon. A **133**, 435 (2018).
[35] A. Billoire, T. Neuhaus, and B. A. Berg, Nuclear Phys. B **413**, 795 (1994).
[36] R. H. Swendsen and J. S. Wang, Phys. Rev. Lett. **58**, 86 (1987).
[37] S. Wiseman and E. Domany, Phys. Rev. E **51**, 3074 (1995).